A CFD APPROACH TOWARDS MODELING BLADE/VORTEX IMPINGEMENT EFFECTS AND BUFFETING OVER AIRFOILS

M. Mamou and M. Khalid
Institute for Aerospace Research, National Research Council Canada
Ottawa, Ontario, Canada, K1A 0R6

Keywords: *airfoil-vortex-interaction, shock wave oscillation, viscous separation*

Abstract

Unsteady flows resulting from airfoil-vortex-interaction (AVI) and a shockwave-boundary-layer-interaction (SBLI) are studied numerically using the Reynolds-averaged Navier-Stokes equations. For the AVI problem, two NACA0012 airfoils are used in tandem. The leading one, pitched down at an angle of attack of 20 degrees, is used to generate a distinct vortex by imposing a shockwave ahead of the airfoil. The second airfoil, pitched up at an angle of attack of 5 degrees, is used to intercept the vortex and undergoes the AVI process. Most of the grid points are distributed along the vortex path in order to avoid numerical dissipation for both cases. The results showed that the interaction of the vortex with the airfoil has notable effects upon the aerodynamic characteristics. For the SBLI problem, the separated unsteady flows resulting from the interaction between a shockwave and the boundary layer are studied. Two test airfoils are considered: the 18% thick circular-arc-airfoil and the BGK No. 1 airfoil. Numerical results demonstrated that the unsteady behaviour of the flow is sensitive to the turbulence models. For instance, the unsteadiness of the flow past the circular-arc-airfoil is accurately predicted by the Spalart-Allmaras and the SST model; however, for the BGK No. 1 airfoil, using the same grid, the SST model predicted steady flows with a stationary shockwave. The Spalart-Allmaras model described the shock oscillation phenomenon well and the results agree with experimental observations.

1 Introduction

The flow past helicopter rotor blades is unsteady, separated and three-dimensional. Even for fixed wing aircraft, separated flows with large pressure fluctuations lead to an unpleasant shaking of the wing and vibrations in the passenger cabin. It is difficult to capture the true physics of such flows using numerical model, especially for the rotor-powered vehicles. This involves integrating state-of-the art expertise in unsteady solution algorithms to incorporate complex grid motion in a Chimera environment, together with the application of advanced turbulence models to resolve tip vortex evolution, and other impingement effects in real time. In order to study this problem in any depth, it is far more convenient to study certain aspects in a two-dimensional model. In this paper two such aspects are considered. The first concerns airfoil-vortex-interaction (AVI), and the second concerns buffeting problems over airfoils.

1.1 AVI problem

The flow field around cross-sections of the two rotor blades responds to the presence of a vortex as it travels past the airfoil. The changes to the basic pressure flow field around the airfoil emanate from the vortex impingement effects with dire noise and vibration implications. Designers have wrestled with blade-vortex-interaction (BVI) problems for decades for simulating the flows on propeller-powered vehicles and other rotorcraft flowfield.

The AVI phenomenon and the resulting acoustic waves have been examined experimentally, [1]-[2], in a conventional shock tube with two airfoils in tandem. The vortex generated by the lead airfoil breaks up as it encounters the leading edge of the aft airfoil, and causes oscillatory flows. Acoustic waves are also generated during the AVI process. The effect of the miss-distance (the distance between a horizontal line passing through the leading edge of the airfoil and a horizontal line passing through the vortex core) on the AVI phenomenon has also been studied for the same type of experiment [3]. The aerodynamic loads were affected considerably when the vortex passes close to the airfoil. The AVI process is simulated numerically using a CFD Euler model with unstructured grids [1], [3] and [4]. The numerical domain, however, was limited to the aft airfoil region and a simplified model was used. The study was performed by planting a vortex ahead of the airfoil. Using a sufficiently high grid density, the flow characteristics agreed qualitatively well with experimental observations [1] when the vortex passes close to the airfoil. A Numerical simulation of the whole process, using two airfoils in tandem, has been performed using the Spalart-Allmaras turbulence model [5]. The generation of a vortex and its interaction with the test airfoil were successfully simulated and a good comparison of the time history of the lift coefficient with experiment results was obtained. There is another study in progress at the Institute for Aerospace Research (IAR) [6] that addresses the vortex blade interaction effects experimentally. It is believed that helicopter blades can be equipped with active self-operational devices that can automatically open and shut to 'swallow' or dampen the vortex impingement effects.

1.2 Buffeting over airfoils

The buffeting phenomenon is related to the dynamic response of aircraft wings or tails to oscillatory loads acting on them. Severe buffeting problems usually occur in the transonic regime. The phenomenon is caused by the interaction of shockwaves with the boundary layer, resulting in self-sustained shock oscillation. The shock oscillation is characterized by a periodic location change over a wing, which affects the aerodynamic forces considerably and causes undesirable vibrations and unpleasant shaking. Recent advances in CFD techniques and high speed computing make it possible to simulate the buffeting phenomenon. An experimental study [7] was conducted to investigate the buffeting problem on an 18% thick circular-arc-airfoil in the transonic regime. The study provided tangible experimental data for CFD code validation. Using different turbulence models and grid sizes [8], a thorough investigation of buffeting over an 18% thick circular-arc-airfoil was performed. The Spalart-Allmaras turbulence model accurately predicted the shockwave oscillation and its frequency. Another buffeting airfoil case was studied experimentally [9], using a BGK No. 1 airfoil at the National Research Council 1.5m × 1.5m trisonic blowdown wind tunnel. Results were obtained in terms of the pressure fluctuation over the airfoil and the oscillation frequency of the shockwave.

The present paper describes a two-dimensional numerical simulation of the problems cited above: the AVI problem past two airfoils in tandem, and the buffeting phenomenon over an 18% thick circular-arc-airfoil and a BGK No. 1 airfoil. Time accurate solutions were obtained using the Spalart-Allmaras and SST turbulence models with adequate grid sizes and time steps. Results are presented in terms of pressure and Mach number contours and the time history of the aerodynamic loads on the airfoils.

2 Problem Description

2.1 AVI problem

The experimental apparatus described in [1] is modeled in the present study. The apparatus consists of a rectangular-cross-section shock tube, in which two NACA 0012 airfoils are placed in tandem. The test area is shown in Figure 1. The distance between the two airfoils is taken to be 5.4 ***c***, where ***c*** is the airfoil chord length of 120 mm. The lead airfoil is used to generate the vortex. The aft airfoil intercepts the vortex and undergoes the AVI process. The angles of attack of the lead and aft airfoils are 20 degrees (nose down) and 5 degrees (nose up), respectively. In the experiment [1], a traveling shockwave is initiated after the breakdown of the diaphragm. This induces a freestream flow, which can be assumed steady for the period of time between 1.6 and 9.1 ms. The flow conditions behind the shockwave are M_∞=0.69 and p_∞=3.278 psi. A distinct vortex is generated at the trailing edge of the lead airfoil when the shockwave interacts with it, as depicted in Figure 1. The vortex is then separated and convected downstream, where it interacts with the aft airfoil.

2.2 Buffeting over airfoils

For the buffeting flow problem, unsteady flows past two airfoils are studied. The first is an 18% thick circular-arc-airfoil at zero incidence. The flow conditions are given in [7] and [8]. The free stream Mach number is 0.76 and the Reynolds number based on the chord length is $Re = 11 \times 10^6$. The second is a BGK No. 1 supercritical airfoil at an angle of attack of 6.066 degrees and a Reynolds number of 20×10^6. The freestream Mach number is 0.746 [9].

3 Numerical Solution

For the AVI problems, the numerical domain is divided into 10 zones using a structured grid to allow parallel processing. A coarse grid of the full configuration is shown in Figure 2. The noncontiguous grid strategy is used in order to distribute a large number of the grid points along the vortex path to avoid numerical dissipation of the vortex. A time accurate solution is obtained using the WIND code with the global Newton iteration procedure [10]. The number of grid points over the computational domain is about one million, and a time step of 5×10^{-7} seconds is adopted. The Spalart-Allmaras turbulence model is used. A maximum normal distance from the walls of $5\times10^{-6}\,\boldsymbol{c}$ is considered to ensure that y^+ is less than 2.5 during the computations. The convergence criterion within each time step is achieved when the maximum global residual of the transport equations is reduced by three orders of magnitude. Parallel processing is performed using three different SGI machines, each one with two CPUs, that are available at the Institute for Aerospace Research.

For the buffeting flows, the grid over the 18% thick-circular-arc-airfoil and the BGK No. 1 airfoil are shown in Figure 3. The computations were performed with a 257x97 mesh with a maximum normal spacing of $4\times10^{-6}\,\boldsymbol{c}$ for the circular-arc-airfoil, and with 537x129 mesh with maximum normal distance of $2\times10^{-6}\,\boldsymbol{c}$ for the BGK No. 1 airfoil. The Spalart-Allmaras (SA) and the shear-stress turbulence (SST) models are used. In both cases, the maximum y^+ is less than 2. The computations are carried out on single C-grid block with the far field located 50 chords away from the airfoils. The Navier-Stokes code uses the upwind scheme for spatial differencing of the convective terms and central differencing for the diffusion terms. Flux limiting is considered to obtain a smooth solution near the shock waves. The fluxes at the grid cell faces are computed using the Roe's flux-difference-splitting scheme. The temporal terms are discretized using the second-order backward differencing schemes and the solution is obtained implicitly by performing sub-iterations within each time step. The chord and the speed of sound are used for non-dimensionalizing the governing equations. The dimensionless time step in the present computations is between 0.001 and 0.01. Convergence within each time step is assumed

when the maximum residual in the discretized equations is decreased by three orders of magnitude.

4 Results and Discussion

4.1 Airfoil-vortex-interaction

The initial conditions used in the tandem airfoils problem are defined by prescribing a shockwave ahead of the lead airfoil. The pressure is low and the flow is motionless downstream of the shockwave. A nearly uniform freestream flow is induced behind the shockwave where the pressure is relatively high. The shockwave is traveling downstream at Mach number of 1.6, and the induced flow behind the shock is at a Mach number of 0.69, as observed in experiment [1].

As soon as the shock impinges upon the lead airfoil, a reflection compressibility wave is generated and propagates in all directions. When the shockwave arrives at the trailing edge of the airfoil, a new and distinct vortex is created, as shown by the pressure contours in Figure 4 (a). The vortex is then separated and convected downstream towards the aft airfoil. Figure 4(b) displays the vortex at the midway point between the lead and the aft airfoil. At this time, the shockwave is at the mid-chord of the aft airfoil. Figure 4(c) shows that a nearly circular compressibility wave is generated when the shock wave impinges on the airfoil.

As the shock wave leaves the trailing edge of the airfoil, the unsteady flows past the two airfoils become more complex, as shown in Figure 5. Owing to the high angle of attack of the lead airfoil, a massive viscous separation is initiated and shockwaves are formed on the lower surface of the airfoil. The compressibility wave that emanates from the lead airfoil is reflected downwards by the upper horizontal wall, it passes across the vortex and strikes the two airfoils. The compressibility wave emanates from the aft airfoil continues to grow, while another weak compressibility wave forms at the trailing edge when the imposed shock wave leaves the aft airfoil. At this time, the vortex is close to the leading edge of the aft airfoil.

When the vortex approaches the aft airfoil, the flow becomes highly unsteady and more complex. As can be seen from the pressure contours in Figure 6, many compressibility waves are generated during the AVI process. The vortex arrives at the leading edge of the airfoil, on Figure 6(a), is located at mid-chord of the airfoil, on Figure 6(b), and is located a quarter chord downstream of the airfoil on Figure 6(c). A qualitative comparison of the results of Figure 6(a) and (c) demonstrates clearly how the presence of a vortex near an airfoil affects the unsteady behaviour of the flow and the generation of many compressibility waves, which are regarded as a source of noise.

Figure 7 illustrates two snapshots of the Mach number contours during the AVI process. The vortex path is at 0.14 chords below the airfoil. Hence, the flow below the lower surface of the airfoil is significantly affected by the presence of the vortex. Despite the positive angle of attack of the airfoil (5 degrees nose up), the high-pressure region is located above the upper surface while the low-pressure region is beneath the airfoil. Since the vortex flow is clockwise, the flow below the airfoil is accelerated and gives rise to different regions of supersonic flow (red color) accompanied by shockwaves. A mild viscous separation is observed on the lower surface.

As expected, the aerodynamic loads of the aft airfoil were considerably affected by the passage of the vortex. The time history of the lift coefficient, C_L, is presented in Figure 8. Experimental results [1] are presented in the same figure for comparison. As the shock wave moves along the airfoil, an induced flow develops over the airfoil and causes the lift to increase progressively. The lift starts to decrease as the compressibility wave that is

reflected from the upper wall strikes the airfoil. It increases again when the compressibility wave separates from the airfoil. As the vortex approaches the airfoil, the lift decreases drastically to C_L = -0.5. A rapid recovery of the lift occurs when the vortex separates from the airfoil. The simulated results agree well with the experimental data. The discrepancy between the present simulations and the experimental results is due to the reflection of compressibility waves from the upper and lower walls, which is weakened in the experiment by incorporating triangular slates on the top and the bottom walls of the shock tube.

4.2 Buffeting over airfoils

Buffeting over an 18% thick circular-arc-airfoil is first considered. The freestream conditions correspond to M=0.76, and Re=**11 × 10^6**, where Re is the Reynolds number based on the airfoil chord length. The solution is obtained using both SA and SST turbulence models. The Mach number contours at different shock locations and the lift coefficient as a function of time are displayed in Figures 9 and 10. The oscillatory flow is characterized by a shockwave motion resulting from the SBLI phenomena. The oscillation is periodic, but the flow patterns are asymmetric. The flow behaviour on the upper side is exactly the same as that on the lower side, but it is shifted in phase by a half period of time. From Figure 9, the results demonstrate the occurrence of an alternating of shockwave-induced and trailing-edge separation. The reduced frequency is k=0.417 for the SA model and 0.422 for the SST model, which is close to k=0.47 predicted in [8] and [9]. For the SST simulation, the SA solution is used for the initial conditions. The lift coefficient amplitude is a little bit reduced, as shown in Figure 10. The maximum lift coefficient obtained with the SA and SST turbulence models is 0.3613 and 0.327 respectively, which are close to those reported in [8] using the SA turbulence model (k=0.361).

The results, for the BGK No 1 airfoil, are presented in Figures 11 and 12. The freestream conditions used are those reported in the experiment [9]: M=0.746 and Re=**20 × 10^6**. The angle of attack is 6.066 degrees. For this case, the experimental data reveal that the shock oscillation occurs on the upper surface of the airfoil. The shock is moving periodically backwards and forwards, and induces separation at its root. This phenomenon is caused by the interaction between the shockwave and the boundary layer. In the experiment [9], the oscillation of the shockwave occurs within a short distance of the mean position. The present numerical results obtained with the SA turbulence model are displayed in Figures 11 and 12. They show that the shock oscillates within a good half chord from the leading edge for the airfoil. The reduced frequency is k=0.586, which is close to the experimental prediction (k=0.537). Using the same grid, same input data and different time step (0.0005 to 0.05), the SST turbulence model always gives a steady-state solution (stationary shockwave with separation). From Figure 12, the lift coefficient amplitude is not constant and the stroke of the shockwave for two successive oscillations is slightly different.

5 Conclusions

In the present paper, a two-dimensional numerical analysis is performed to study the AVI phenomenon within a shock tube in which two NACA 0012 airfoils are mounted in tandem, and the buffeting flows over an 18% thick circular-arc-airfoil and a BGK No. 1 airfoil. The solution is obtained by solving the RANS equations, using different turbulence models (SA and SST). For the AVI phenomenon, the vortex is generated at the trailing edge of the lead airfoil and convected downstream where it interacts with the aft airfoil. The study showed that the presence of a vortex in close proximity to an airfoil has noticeable effects upon the flowfield surrounding the airfoils and on the aerodynamic loads. The interaction of the vortex with the airfoil generates

compressibility waves that are responsible for various noise issues associated with rotor-blade flows.

For the buffeting problem, a numerical simulation of transient turbulent flows that are induced by shockwave and boundary layer interactions is performed. For buffeting over an 18% thick circular-arc airfoil, the results agreed well with experimental data for both Spalart-Allmaras and SST turbulence models. The accuracy of the numerical results is sensitive to the grid refinement, time step and turbulence model. For the BGK No 1 airfoil, the SST model is felt to predict the unsteadiness of the flows. Using different initial conditions, the model always leads to steady-state solution with a stationary shockwave.

Acknowledgements

The authors are grateful to the Canadian Department of National Defence for their financial support, and to the NPARC alliance for permission to use their WIND code. The authors would like to thank Dr. McIlwain for reviewing this paper and providing constructive comments.

References

[1] Sobieraj G, Piechna J, Selerowicz W and Szumowski A P. Effect of angle of attack on the airfoil-vortex interaction. *The Arch. Mech. Eng., XLV*, Vol. 1., 1998.

[2] Kaminski W S and Szumowski A P. Acoustic effects of parallel vortex-airfoil interaction. *Journal of Sound and Vibration*, Vol. 183, No. 2, 1995.

[3] Selerowicz W, Sorbieraj, G and Szumowski A P. Effect of miss-distance on the airfoil-vortex interaction: Experiment. *Arch. Mech*., Vol. 50, No. 1, Warszawa, 1998

[4] Piechna J and Szumowski A P. Effect of miss-distance on the airfoil-vortex interaction: Numerical study, *Arch. Mech*., Vol. 50, No. 1, Warszawa, 1998.

[5] Mamou M, Khalid M and Xu H. Unsteady flows past two airfoils in tandem and airfoil-vortex-interaction. *Canadian Aeronautics and Space Journal, under press,* 2002.

[6] Zimcik D. "Development of helicopter rotor individual blade control techniques for combined noise and vibration reduction, Institute for Aerospace Research, NRC, Progress Report, February 2001.

[7] McDevitt J. Supercritical flow about thick circular-arc-airfoil. NASA TM-78549, 1979.

[8] Rumsey C L, Nanetrik M D, Biedron R T, Melson N D and Parlette E B. Efficiency and accuracy of time-accurate turbulence Navier-Stokes computation. Computers & Fluids, Vol. 24, No. 2, pp 217-236, 1996.

[9] Lee B H K. Oscillatory shock motion caused by transonic shock boundary-layer interaction. *AIAA Journal*, Vol. 28, No. 5, 1989.

[10] The NPARC Alliance, *NASA Glenn Research Center, Cleveland, Ohio*, WIND Code manuals

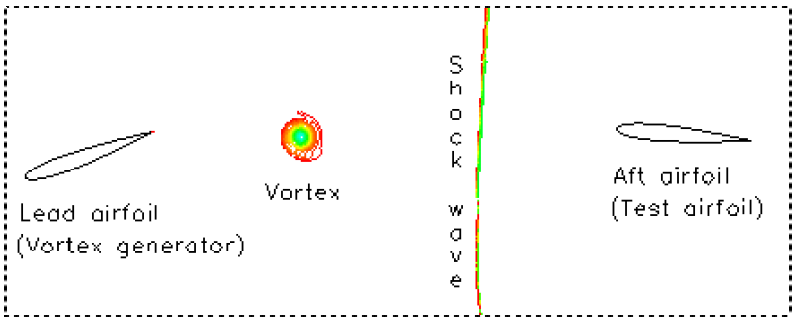

Figure 1: Schematic diagram of vortex generation by the passage of a shockwave.

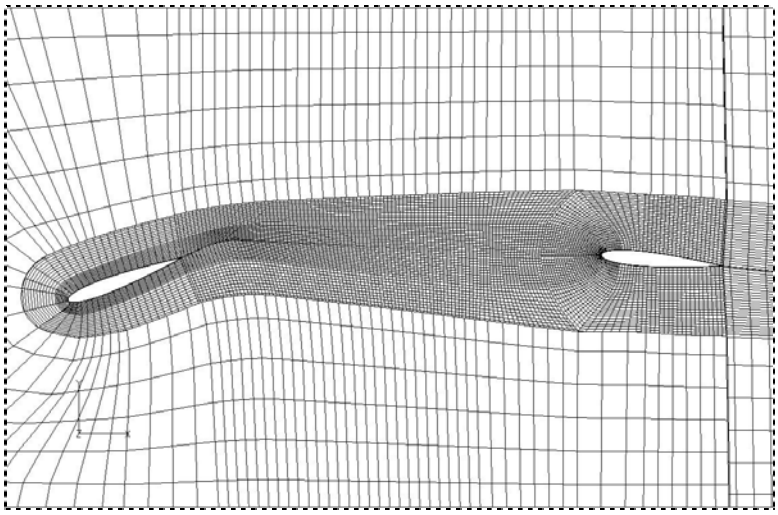

Figure 2: Grid used for the AVI problem. The mesh has been coarsened; the actual grid size is ten times smaller.

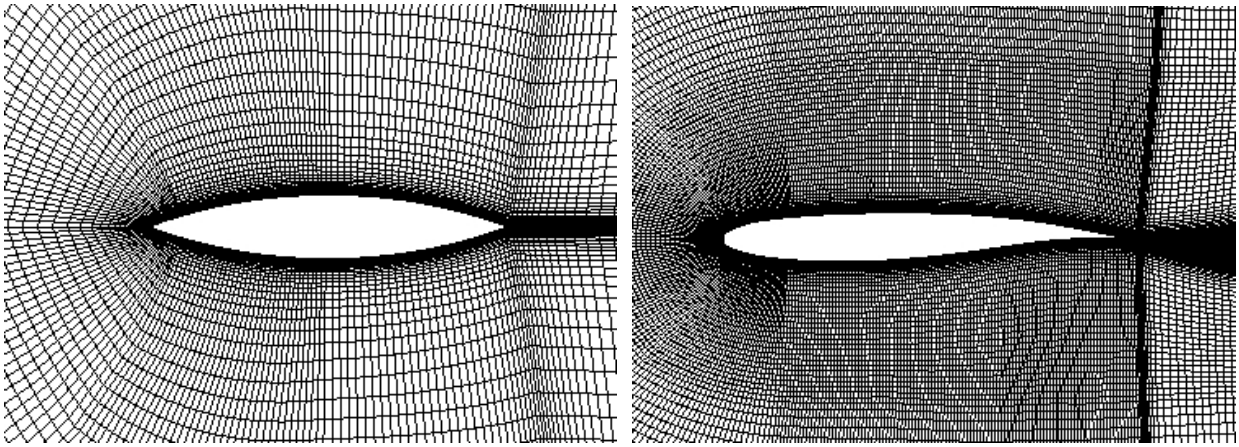

a) b)

Figure 3: Grid used for buffeting flows over a) an 18% thick circular-arc-airfoil, and b) a BGK No. 1 airfoil.

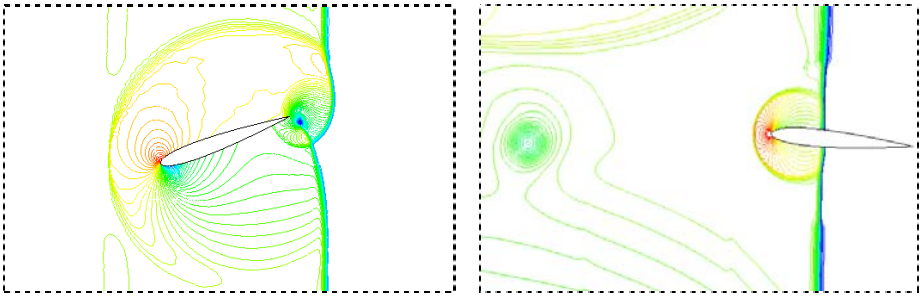

a) b)

Figure 4: Pressure contours: a) vortex generation by the lead airfoil, b) vortex traveling to the aft airfoil.

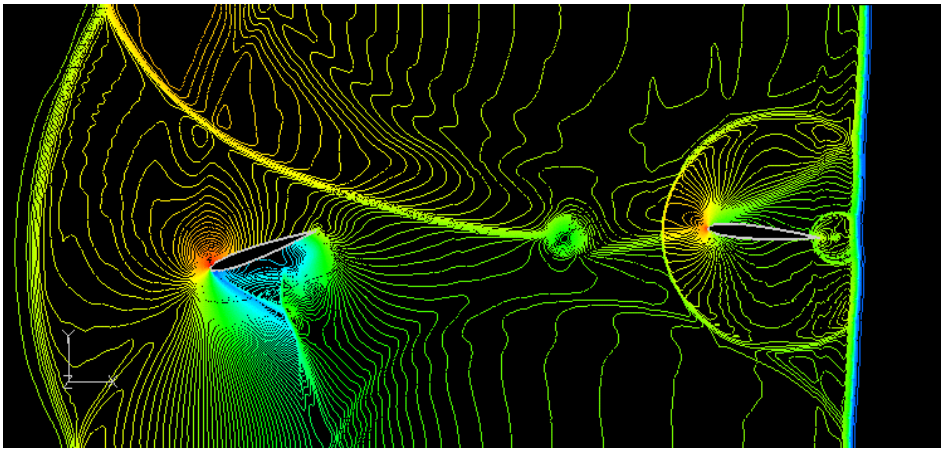

Figure 5: Global view of the pressure contours when the vortex is in close proximity to the aft airfoil.

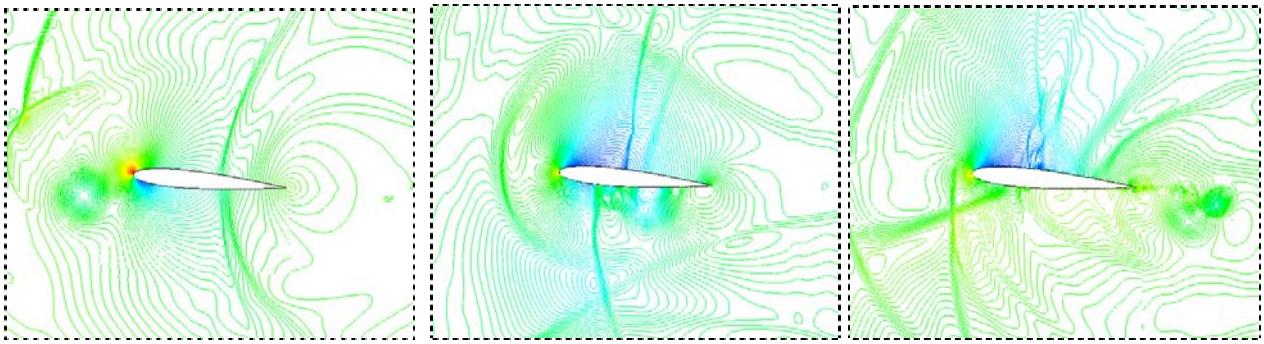

Figure 6: Pressure distribution contours for the airfoil-vortex-interaction process with: a) the vortex is ahead of the airfoil, b) the vortex located at the mid-width of the airfoil, and c) after the vortex has separated from the airfoil.

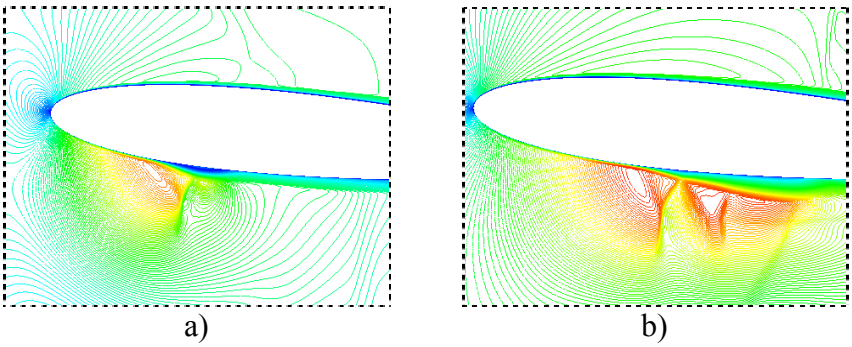

Figure 7: Two snapshots of the Mach number contours during the AVI process.

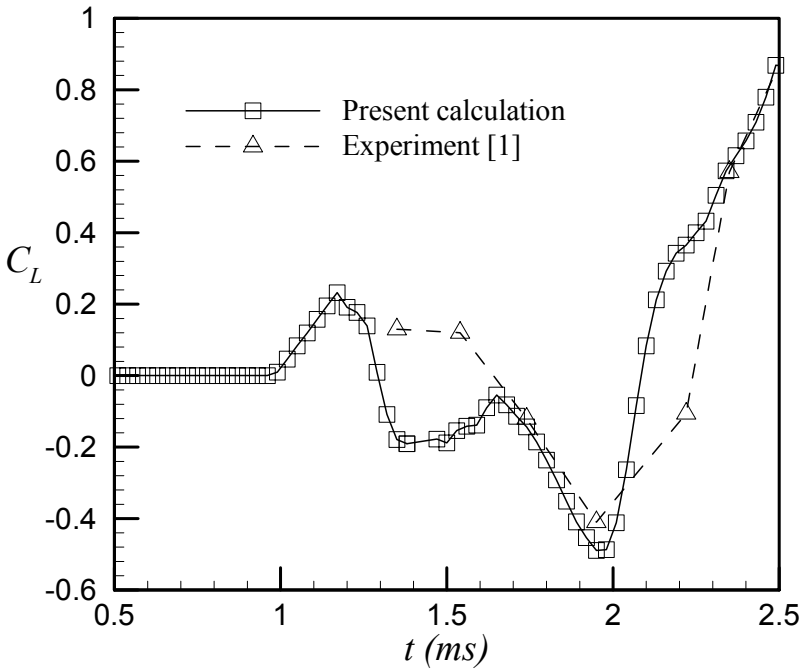

Figure 8: Time history of the lift coefficient C_L for the aft airfoil.

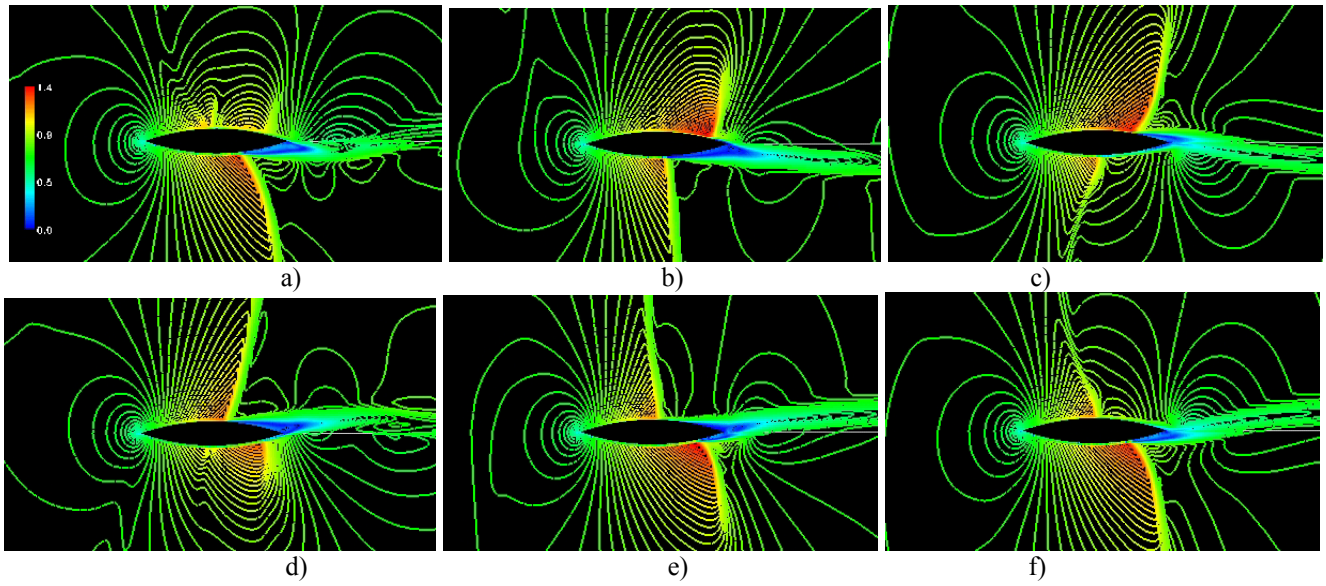

Figure 9: Mach number contours for the 18% thick circular-arc-airfoil. M=0.76 and Re=11 × 10^6.

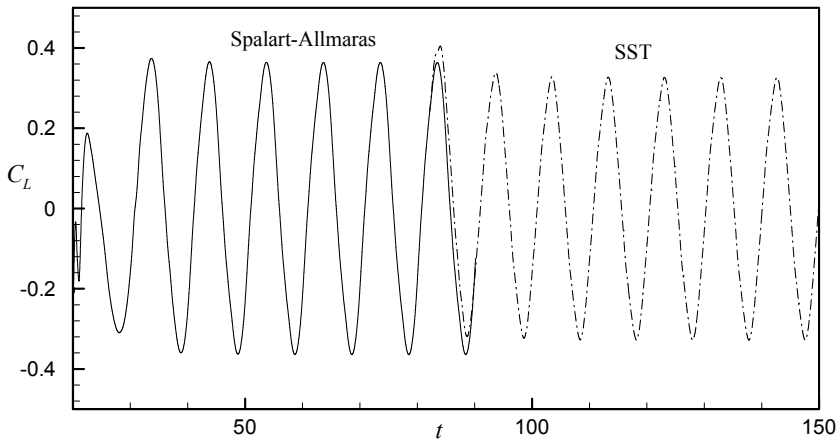

Figure 10: Time history of the lift coefficient for an 18% thick circular-arc-airfoil using the SA and SST turbulence models.

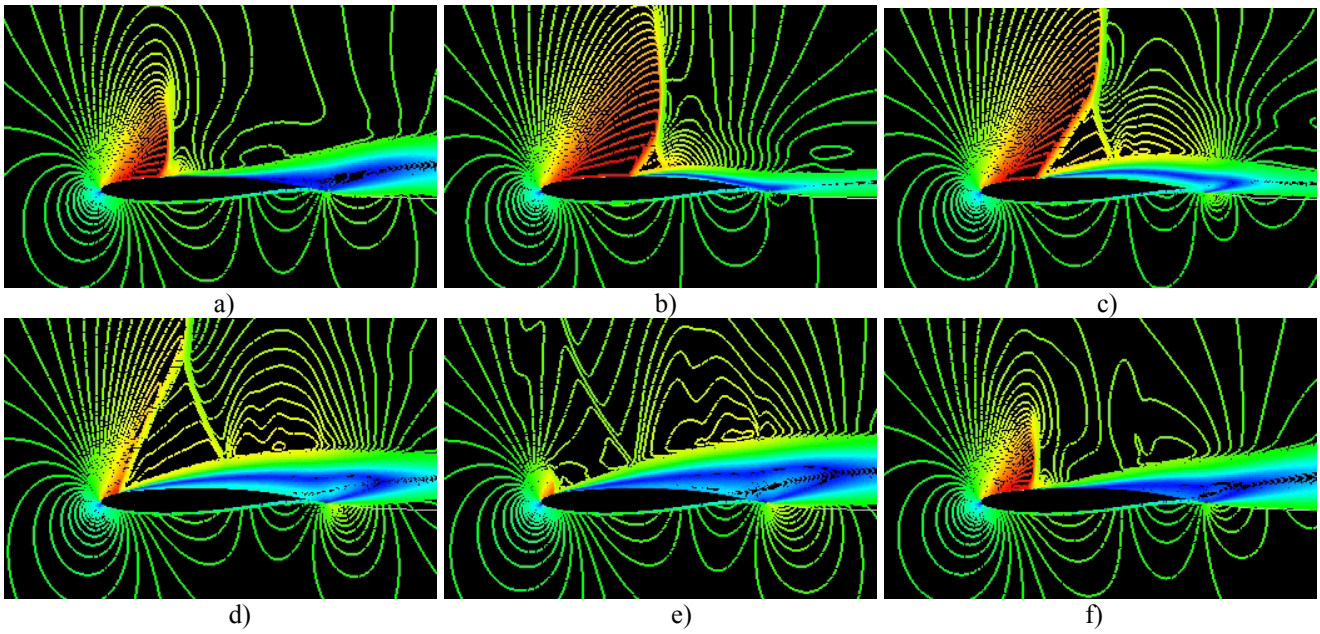

Figure 11: Mach number contours for the BGK No. 1 airfoil, M=0.746, AOA=6.066 degrees and Re=11 × 10^6.

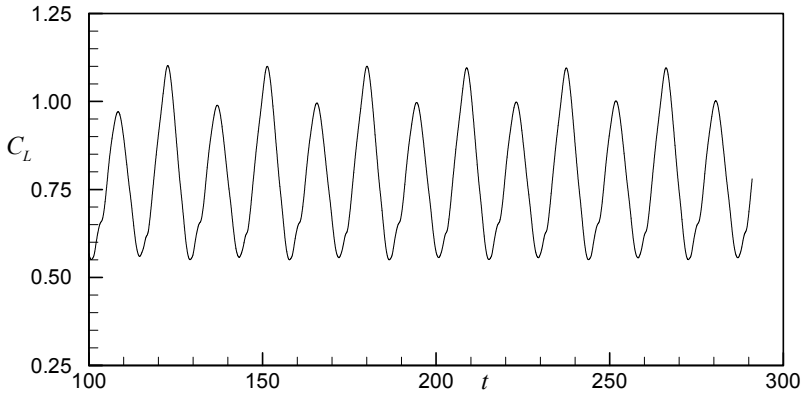

Figure 12: Time history of the lift coefficient for the BGK No. 1 airfoil using the SA turbulence model.